

21. Banakar, V. K. *et al.*, Indian summer monsoon forcing on the deglacial polar cold reversals. *J. Earth Syst. Sci.*, 2017; doi:10.1007/s12040-017-0864-5.
22. Sinha, A. *et al.*, Variability of Southwest Indian summer monsoon precipitation during the Bølling- Allerød. *Geology*, 2005, **33**, 813–816.
23. Deplazes, G. *et al.*, Links between tropical rainfall and North Atlantic climate during the last glacial period. *Nat. Geosci.*, 2013, **6**, 1–5.
24. Ponton, C. *et al.*, Holocene aridification of India. *Geophys. Res. Lett.*, 2012, **39**, 1–6.
25. Nishimura, M. *et al.*, Paleoclimatic changes on the southern Tibetan Plateau over the past 19,000 years recorded in Lake Pumoyum Co and their implications for the southwest monsoon evolution. *Palaeogeogr., Palaeoclimatol., Palaeoecol.*, 2014, **396**, 75–92.
26. Staubwasser, M. *et al.*, Climate change at the 4.2 ka BP termination of the Indus Valley Civilization and Holocene South Asian monsoon variability. *Geophys. Res. Lett.*, 2003, **30**; doi:10.1029/2002GL016822.
27. Dileep Kumar, M., *Biogeochemistry of the North Indian Ocean*, Indian Academy of Sciences, Bangalore, 2006.
28. Sastri, V. V. *et al.*, Stratigraphy and tectonics of sedimentary basin on East coast of peninsular India. *AAPG Bull.*, 1973, **57**, 655–678.
29. Purnachandrarao, V. and Kessarkar, P. M., Geomorphology and geology of the Bay of Bengal and the Andaman Sea. In *The Indian Ocean: A Perspective* (eds Sengupta, R. and Desa, E.), Balakema Publ., 2001, vol. 2, pp. 818–868.
30. Ramkumar, M. *et al.*, Deltaic sedimentation during Cretaceous period in northern Cauveri basin, South India: facies architecture, depositional history and sequence stratigraphy. *J. Geol. Soc. India*, 2004, **66**, 81–94.
31. Anitha, G. *et al.*, Shallow geological environment of Krishna-Godavari offshore, Eastern Continental margin of India as inferred from the interpretation of sparker data. *J. Earth Syst. Sci.*, 2014, **123**, 229–342.
32. Alappat, L. *et al.*, Chronology of Cauvery delta sediment from shallow subsurface cores using elevated temperature post-IR IRSL dating of feldspar. *Geochronometria*, 2010, **37**, 37–47.
33. Subramanian, V. *et al.*, Chemical composition of river sediments from the Indian subcontinent. *Chem. Geol.*, 1985, **48**, 271–279.
34. Dekov, M. *et al.*, Chemical composition of sediment and suspended matter from the Cauveri and Brhamaputra rivers (India). *Sci. Total Environ.*, 1998, **212**, 89–105.
35. Dickens, G. R. and Owen, R. M., Late Miocene–Early Pliocene manganese redirection in the central Indian Ocean: expansion of the intermediate water oxygen minimum zone. *Palaeoceanography*, 1994, **9**, 169–180.
36. Schenau, S. J. *et al.*, Oxygen minimum zone controlled Mn redistribution in Arabian Sea sediments during the late Quaternary. *Palaeoceanography*, 2002, **17**; doi:10.1029/2000PA000621.
37. Miriyala, P. *et al.*, Increased chemical weathering during the deglacial to mid-Holocene summer monsoon intensification. *Sci. Rep.*, 2017; doi:10.1038/srep44310.

ACKNOWLEDGEMENTS. We thank MoES and CSIR for funding support, and Anita Garg, DeMartino Mitizi and G. Parthiban for analytical help. B. Nagender Nath provided the sediment core. The meticulous review and constructive comments of an anonymous reviewer were of great help.

Received 2 April 2017; revised accepted 5 January 2018

doi: 10.18520/cs/v114/i09/1940-1946

Multiple regression analysis of geoelectric imaging and geotechnical site investigation test results

Rambhatla G. Sastry^{1,*}, Sumedha Chahar¹ and Mahendra Singh²

¹Department of Earth Sciences, and

²Department of Civil Engineering, IIT Roorkee, Roorkee 247 667, India

Geotechnical site characterization through non-invasive and cost-effective electrical resistivity imaging (ERI) and induced polarization imaging (IPI) offers promise compared to conventional point-geotechnical site investigations (standard penetration test, SPT), for which a basic understanding of factors (grain size (sand, fines) and water content) influencing them is needed. Here we perform a multiple regression analysis of ERI, IPI and SPT results in a site investigation at Lucknow, India. The results show that grain size and water content influence both chargeability and SPT values in a similar manner, while resistivity values are affected differently with a low RMS prediction error for chargeability.

Keywords: Geoelectronic imaging, geotechnical site characterization, multi-regression analysis, grain size, water content.

GEOMECHANICAL properties of near surface soils are routinely estimated through analysis of soil samples and invasive geotechnical testing that could include, for example, the standard penetration test (SPT), static cone penetration test (SCPT) and dynamic cone penetration test (DCPT)^{1,2}. Although these geotechnical tests provide high-resolution data to geotechnical engineers, their acquisition is fraught with heavy budgets as well as invasive and time-consuming methodologies. Furthermore, SPT and SCPT are not feasible for hard strata at shallow depths^{1,2}, but knowledge of geomechanical properties to sufficient depths is needed for major civil constructions. The possibility of predicting site geotechnical test results through a conjunctive use of geoelectrical (electrical resistivity imaging (ERI) and induced polarization imaging (IPI)) and few geotechnical data was explored³. Electrical data and SCPT results to delineate the subsurface lithological units were used⁴. It is well known among the geotechnical community that the SPT-N value is directly proportional to grain size and clay content, and inversely proportional to porosity and water content^{1,2,5}. However, the relationship between geotechnical parameters and geophysical measurements has been studied by only a few researchers. Resistivity of earth materials is inversely proportional to porosity, clay content and water content whereas

*For correspondence. (e-mail: rgssl1fes@iitr.ac.in)

it is directly proportional to grain size of rock matrix and air content in the vadose zone⁶. So, it would seem logical that electrical measurements could be used to investigate the same rock and soil properties that influence geotechnical measurements. These overlapping soil properties – grain size and water content are referred to as ‘jointly influencing parameters’⁷. A correlation between resistivity and SPT blow count has been reported based on correlation coefficients for different soil types⁸. Electrical resistivity values are affected by geotechnical soil properties (void ratio, grain size, density, Atterberg limit, porosity and moisture content)⁹. Using scatter plots, a simple linear regression analysis was performed to find the correlation between formation strength parameters (friction angle, cohesion, moisture content and plasticity index) and resistivity^{10,11}. Linear and multiple regression analyses were also carried out to predict formation strength parameters (friction angle and cohesion) by considering resistivity and moisture content as independent parameters.

In view of the above, there is an urgent need for a comprehensive study on the influence of different soil parameters (grain size (sand and fines) and water content) on both geoelectrical and geotechnical measurements. Sand and shale/fines refer to standard particle size distribution within subsurface soil mass¹². In the present study, we performed a combined multiple regression analysis of both geoelectric (ERI/IPI) and geotechnical (SPT) datasets acquired at a study region in Lucknow, Uttar Pradesh, India, with a prime objective of identifying the jointly influencing parameters⁷. Our results indicate that the presence of sands, fines and water content in the subsurface influences IP chargeability and SPT-N predominantly linearly, while it affects the resistivity nonlinearly; the extent of the exact influence is guided by local near-surface lithological variations. Thus, this study will provide a basic logic to the conjunctive use of non-invasive and cost-effective geoelectric imaging with minimal deployment of invasive geotechnical testing of a project site.

Figure 1 shows the site location of the study region along with different field geoelectrical profiles and SPT boreholes. For illustration of our methodology, we consider profile A–B (ERI/IPI) along with the nearby SPT boreholes. ERI and IPI data are processed using PROSYS II and interpreted using RES2D INV¹³.

Our study region is located in the Gomti River basin, which is a part of the Indo-Gangetic Alluvial Plains (IGP) of area of 700,000 sq. km. Gomti is the major tributary of the Ganga. It is a rainfed river with its entire drainage in the Ganga plain¹⁴. The morphological features of the IGP include terraces, terminal fans/plains associated with rivers, eolian ridge, alluvial ridge, piedmont alluvial plain and remnants of old Ganga plain¹⁵. The terminal fans include those of Sitapur-Lucknow. The Gomti alluvial ridge is a prominent feature with a relief of 4–6 m

compared to surrounding units. At present, the Gomti River incises the Gomti alluvial ridge. The outer region of the ridge is typically composed of loam/silt size sediments and inner region is coarse sandy, as a result of soil development in the outer part. Faults have played an important role in soil development, notably Gomti fault, Ghaghara fault, Lucknow fault besides many others identified by remote sensing, drainage pattern and digital elevation model studies^{15–17}. The Gomti River is confined to the Gomti fault and it is observed that tectonics control the soil distribution¹⁵.

The Young Sitapur–Lucknow Fan¹⁵ is dated 6.00 ± 1.22 ka and the Young Gomti Plain¹⁵ is around 6.69 ± 0.73 ka (using luminiscence dating). The remnants of old Ganga plain and Gomti alluvial ridge formed by a large river are overlain by soils with ages of 11–15 ka and

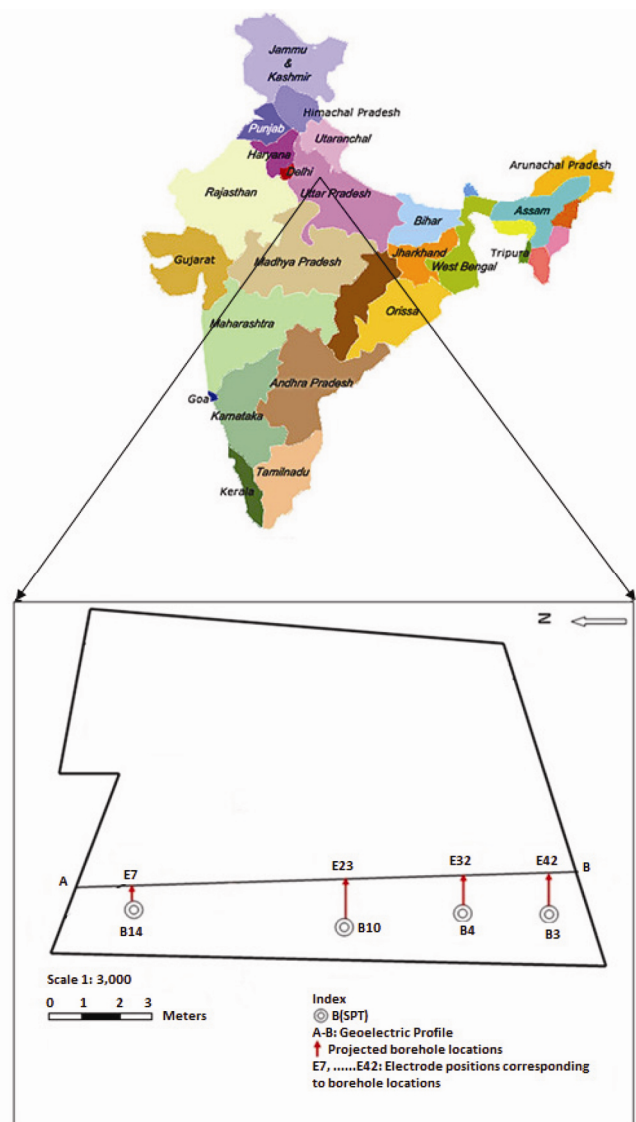


Figure 1. Site location map indicating geoelectric profiles – electrical resistivity imaging (ERI) and induced polarization imaging (IPI) and geotechnical tests – standard penetration test (SPT) locations.

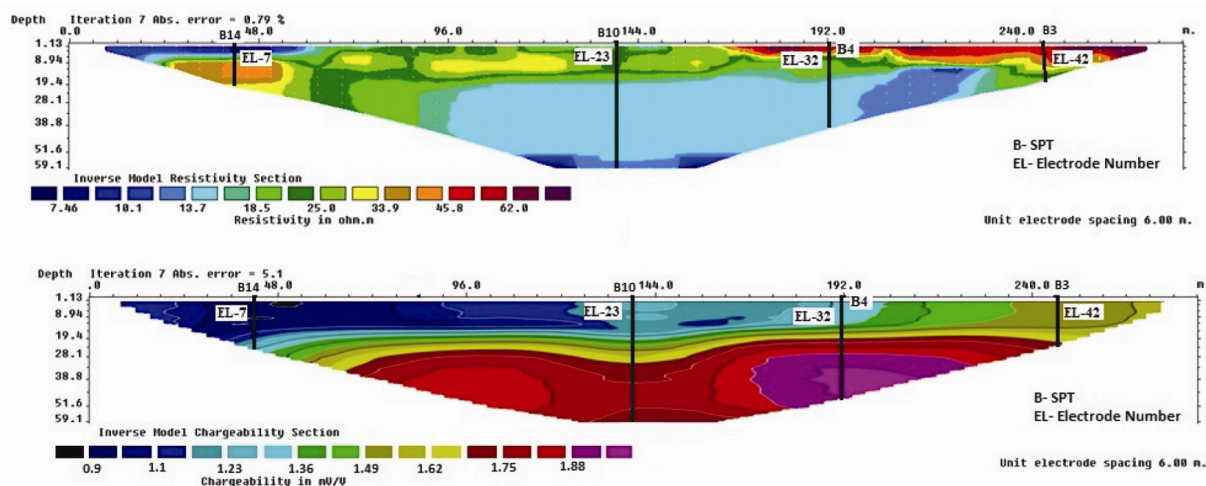


Figure 2. Inverted resistivity (true resistivity) and IP chargeability (true chargeability) sections along profile *A–B* (see Figure 1).

underlain by fluvial deposits suggesting that the interfluvial was probably connected to the major bounding rivers prior to ~ 15 ka (ref. 15). The activity of various segments of different incipient transverse normal faults at different times during 10^5 ka, combined with dry sub-humid/semi-arid climate produced different terminal fans by small ephemeral streams, on which soils started developing¹⁵. Repeated tilting of large blocks in the same direction led to shifting of rivers in the down tilt-direction and soil development in the up-tilt direction¹⁵. The pedogenic response to neotectonics suggests that upliftment of blocks caused a break in sedimentation and initiation of pedogenic activity under prevailing climate¹⁶. In general, the IGP soils are micaceous, but some soils with vertic characters are smectitic¹⁶. They were formed in alluviums derived from the Himalaya and cratonic rocks respectively. The thickness of alluvium varies between 4000 and 6000 m (ref. 17). Only fine-grained sediments are transported and deposited in this region. On the basis of surface and subsurface exploration carried out by various agencies, fine sand, silt, and clay have been recognized as major lithologies.

The ERI and IPI data were acquired using SYSCAL Jr 48 electrode system with a 6 m electrode separation along profile *A–B* (Figure 1) using Wenner–Schlumberger configuration¹⁸. This type of arrangement is a hybrid between Wenner and Schlumberger arrays. It is moderately sensitive to both horizontal and vertical structures¹⁹. Figure 2 shows inverted resistivity and IP chargeability images.

The geotechnical studies made according to standards include SPT-N data acquisition from four boreholes, laboratory studies of collected undisturbed soil samples from boreholes, implementation of appropriate corrections to SPT data and preparation of lithologs for each borehole¹². Table 1 shows a borehole B3, which includes lithology according to IS classification¹², all independent input variables and one dependent function, SPT-N. The over-

burden and dilatancy corrections necessary for field-observed SPT data have been applied¹².

In Figure 2, the four SPT boreholes have been projected onto geoelectric profile *A–B*. SPT-N values were procured systematically with a high resolution in multiples of 0.75 m depth-wise in a linear fashion. The soil samples were also collected at the same depth. They were analysed for grain size (sand and fines content), water saturation and lithology. However, the true resistivity (inverted apparent resistivity) and chargeability logs at the projected SPT borehole positions are in a nonlinear depth scale¹⁹. So, any further statistical analysis of these different datasets needs a common depth-scale basis for all of them. Here, we have chosen discrete 0.75 m as depth-wise sampling interval for all datasets. To achieve this objective, we implemented cubic spline interpolation scheme²⁰ to obtain new datasets (SPT-N, resistivity, chargeability, grain size distribution (sand and fines %) and water content %)²⁰. For non-dimensional stacks (normalized data) of these depth profiles for each borehole (B3, B4, B10 and B14), the relevant discrete data values were divided by their respective maxima.

Multiple regression analysis was done to generate a relationship between independent and dependent variables²¹. The adjusted R^2 is normally used if more than one independent variable exists and it takes into account the sample size. Standard error is the usual standard deviation. Indeed, normalization is not a necessary step for any statistical data analysis like multi regression analysis, but it will help in easy interpretation. It is to be noted that for normalization we took the highest value for the respective discrete geoelectric and geotechnical data (SPT-N, resistivity, chargeability, grain size (sand and fines) and water content).

Next, the factors (independent variables) that affect both the geoelectric and geotechnical data were identified. Here, we chose grain size (sand and fines) and water

Table 1. Litholog (formation parameters) details of standard penetration test borehole, B3 using geotechnical laboratory measurements of undisturbed samples

Depth (m)	IS classification	Grain size analysis		Natural water content (%)	Depth (m)	SPT-N (at 1500 mm depth interval)
		Sand (%)	Fines (%)			
1.5	ML (NP)	19.4	80.6	20.7	1.5	21.5
3	SM (NP)	72.5	27.5	13.3	3	12
4.5	SM (NP)	60.5	39.5	14.6	4.5	11.8
5.25	SM (NP)	81.5	18.5	22.7	6	15.7
6	SM (NP)	82	18	22.4	7.5	16.8
7.5	SM (NP)	76.5	23.5	21.7	9	21.6
8.25	SP-SM	85	8.5	20.1	10.5	21.1
9	SP-SM	83.5	6	19.4	12	22.9
10.5	SP-SM	82.5	6	20	13.5	44
11.25	GP	13	2	4.5	15	35
12	SM (NP)	65	22.5	16.7	16.5	31.0
13.5	ML	2	68.5	19.8	18	29.3
15	CL-ML	3	69.5	15	19.5	29.7
17.25	ML (NP)	23	75	23.1	21	30.7
18	ML (NP)	22	76.5	22.9	22.5	32.8
20.25	ML (NP)	23.5	76.5	23.4	24	37.3
21	ML (NP)	27	73	25.2	25.5	70.4
23.25	ML (NP)	49	51	22.8	27	102.0
24	SM (NP)	58.5	41.5	25.4	28.5	104.2
27	CL	12	88	22.7	30	105.0
30	CL	7.5	92.5	25.2		

saturation as influencing parameters for normalized SPT-N, resistivity and chargeability, and carried out multi-regression analysis. We have also implemented a multi-collinearity test among the influencing independent variables through the method of correlation coefficients to fix the real set of independent parameters. Hereafter, we will refer to SPT-N, resistivity and chargeability as observed datasets and outcome of multiple regression analysis as predicted data. The RMS error between the observed and predicted values (ERI/IPI and SPT) ascertains the influence of factors (independent parameters) affecting them.

Depth-wise sampled resistivity (21 values), chargeability (21 values) and SPT-N (38 values) for borehole B3 were normalized and they formed the input-dependent functions along with independent variables (Table 1) to the multi-regression analysis module. Similar effort was made for other boreholes like B4, B10 and B14 (Figure 1). Tables 2 and 3 summarize multiple regression results (obeying multi-collinearity) of all boreholes B3, B4, B10 and B14 (Figure 1). Figure 3 shows multiple regression results (obeying multi-collinearity) for borehole B3. In Tables 2 and 3, in first column dependent variables are included while in second–sixth columns the weighting coefficients of free variables, their standard error, t-statistics and probability value at 95% confidence upper and lower bounds are included borehole-wise. The remarks appearing in the tables are self-explanatory.

Usually, electrical polarizability is expressed in mV/V and chargeability in mS. However, the industrial software

(RES2DINV) has provided chargeability in polarizability units (Figure 2) by undertaking proper internal calculations. As we have utilized normalized datasets (resistivity, chargeability and SPT-N), we can expect their numerical values up to the sixth decimal place (normalized values are not included here), and by no means can one assume that original datasets are measured to the same accuracy.

Figure 4 is a stack plot showing normalized SPT, resistivity, chargeability, grain size (sand and fines) and water content logs corresponding to borehole B3. Respective normalizing factors, mean and standard deviation are also shown in the figure. A cursory examination of these stack plots reveals that trend of SPT-N values follows that of fines. Further, a simultaneous decrease of resistivity beyond 6 m depth and increase of chargeability clearly emphasize the influence of fines on IP chargeability and SPT-N, as SPT-N behaviour is closely linked up with shear resistance of the soil irrespective of grain size (sand or fines). The water saturation plot in the depth range 10.5–17.25 m closely follows that of sand.

We have adopted a simple multi-regression analysis for fixing the role of practically quantifiable independent parameters (grain size and water saturation) on dependent functions (SPT-N, ERI and IPI). Multi-collinearity analysis has been implemented to choose the independent parameters among sand, fines and water content. Accordingly, two sub-cases involving sand and water content (case 1), and fines and water content (case 2) were considered. Even though water salinity could be another independent

RESEARCH COMMUNICATIONS

Table 2. Multiple regression analysis output for electrical resistivity imaging (ERI), induced polarization imaging (IPI) and SPT results for boreholes B3, B4, B10 and B14 by considering sand and water content as influencing independent parameters (multicollinearity – case 1)

Borehole location		B3	B4	B10	B14
IPI (true chargeability inversion absolute error = 5.1%)	Sand (x_1) weights	-0.084	-0.303	-0.141	0.035
	Fines (x_2) weights	-	-	-	-
	Water content (x_3) weights	0.079	0.306	0.613	0.031
	Sts (P -value ≤ 0.05)	S, W	W, S	W, S	S, W
	Ad R^2 (%)	82.7	48.4	26	40.4
	Remarks	1	1	1	1
ERI (true resistivity inversion absolute error = 0.79%)	Sand (x_1) weights	0.308	0.371	0.145	-0.466
	Fines (x_2) weights	-	-	-	-
	Water content (x_3) weights	-0.417	-0.671	-0.796	0.351
	Sts (P -value ≤ 0.05)	W, S	W, S	W	-
	Ad R^2 (%)	37.7	40.5	13.1	16.7
	Remarks	1	1	2	2
SPT	Sand (x_1) weights	-0.227	-0.637	-0.501	-0.120
	Fines (x_2) weights	-	-	-	-
	Water content (x_3) weights	0.211	-0.546	1.007	-0.048
	Sts (P -value ≤ 0.05)	S, W	S, W	W, S	-
	Ad R^2 (%)	78.4	62.7	56	5.1
	Remarks	1	1	1	2

Sts, Statistically significant factors; Ad R^2 , adjusted R^2 ; S, sand; W, Water content. Remarks: (1) High adjusted R^2 -value and linear multiple regression analysis is reliable. (2) Low adjusted R^2 – value and linear multiple regression analysis is rejected.

Table 3. Multiple regression analysis output for ERI, IPI and SPT for boreholes B3, B4, B10 and B14 by considering fines and water content as influencing independent parameters (multi-collinearity – case 2)

Borehole location		B3	B4	B10	B14
IPI (true chargeability inversion absolute error = 5.1%)	Sand (x_1) weights	-	-	-	-
	Fines (x_2) weights	0.100	0.324	0.210	-0.014
	Water content (x_3) weights	0.004	0.268	0.740	0.015
	Sts (P -value ≤ 0.05)	F	F, W	W, F	-
	Ad R^2 (%)	67.8	45.7	38	1.9
	Remarks	1	1	1	2
ERI (true resistivity inversion absolute error = 0.79%)	Sand (x_1) weights	-	-	-	-
	Fines (x_2) weights	-0.220	-0.407	-0.240	-0.072
	Water content (x_3) weights	-0.166	-0.631	-0.958	0.706
	Sts (P -value ≤ 0.05)	F	W, F	W, F	-
	Ad R^2 (%)	6.7	40.3	21.6	5.4
	Remarks	2	1	2	2
SPT	Sand (x_1) weights	-	-	-	-
	Fines (x_2) weights	0.227	0.666	0.627	0.046
	Water content (x_3) weights	0.014	-0.636	1.303	0.010
	Sts (P -value ≤ 0.05)	F	F, W	W, F	-
	Ad R^2 (%)	42.5	57.9	67	-7.3
	Remarks	1	1	1	2

F, Fines. Remarks: (1) High adjusted R^2 -value and linear multiple regression analysis is reliable. (2) Low adjusted R^2 value and linear multiple regression analysis is rejected.

parameter, its inclusion is not justified as it does not influence SPT-N. Further, in our case of a small number of independent parameter sets, it is not worthwhile to use more sophisticated analyses like eigen function–eigen value or principal component.

For multi-collinearity test, the correlation coefficients (not included here) of different soil parameters like grain

size (sand and fines) and water content demonstrate that for all cases, sand and fines are highly correlated (correlation coefficient >0.8), which indicates the presence of multi-collinearity between these variables. However, in this study all the three variables (grain size (sand and fines) and water content) are important. By accepting multi-collinearity results, we studied multiple regression

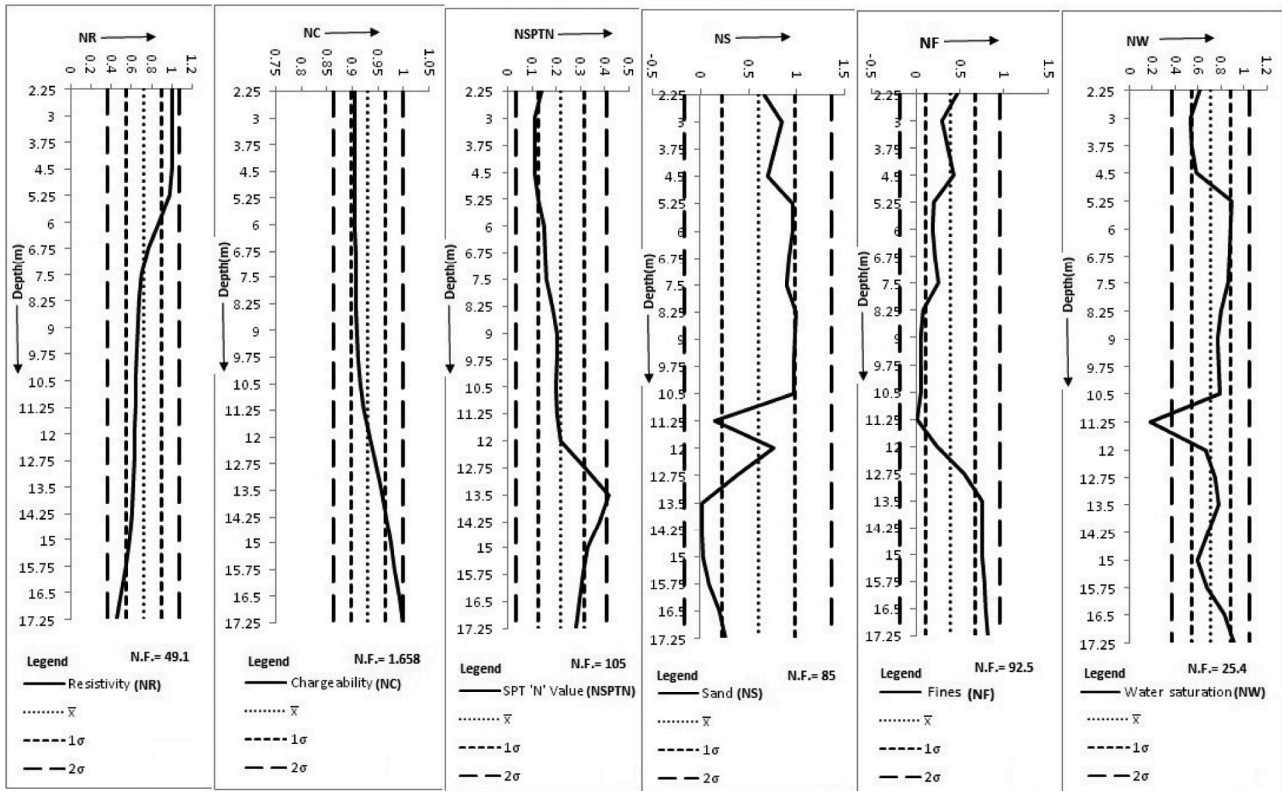


Figure 3. Stack of normalized plots of dependent (SPT-N, resistivity, chargeability) and independent (sand, fines and water content) variables for borehole location B3 profile on A-B (see Figure 1).

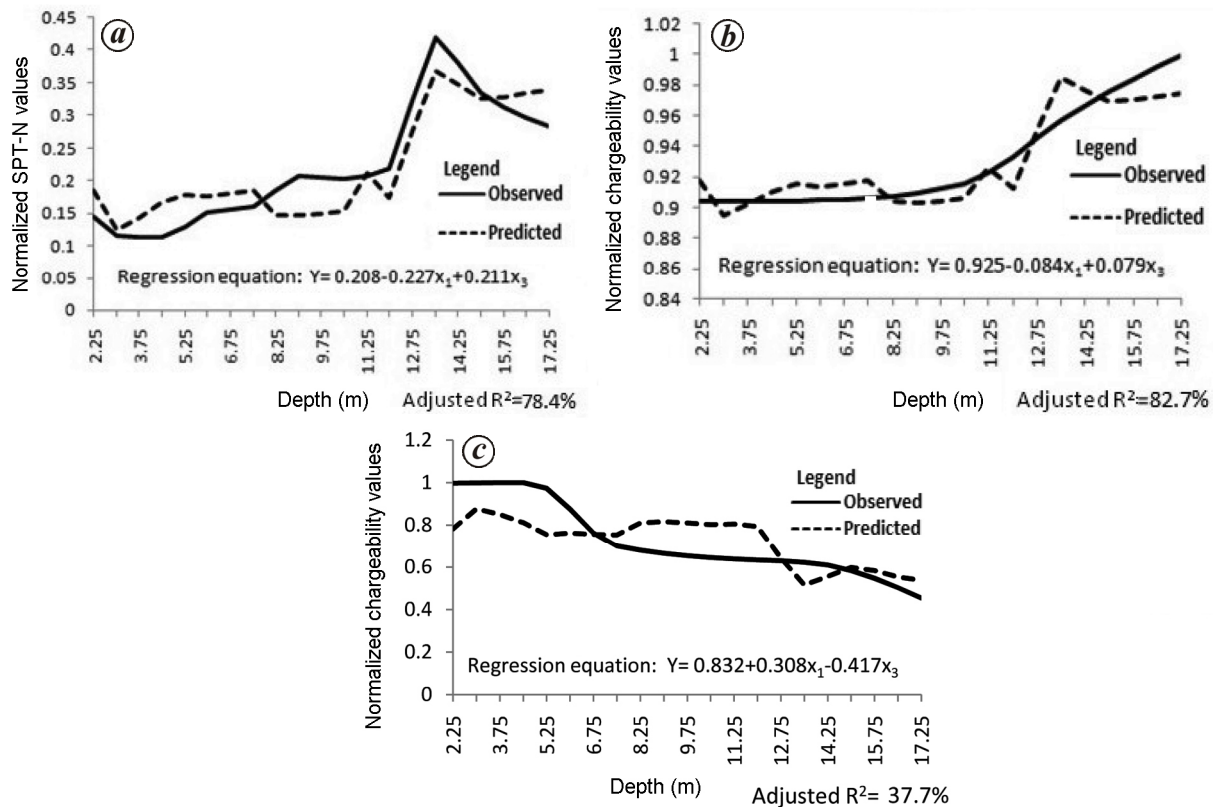


Figure 4. Observed and predicted logs for borehole location B3 through multiple regression analysis considering sand (x_1) and water content (x_3) as independent parameters for profile A-B (multi-collinearity – case 1): a, SPT-N value; b, chargeability; c, resistivity.

in case of sand and water content, and fines and water content separately (Tables 2 and 3). From, scrutiny of different borehole results summarized in Tables 2 and 3, the following points emerge: (1) Fines (clay) and water content have positive contribution, whereas sand has negative contribution in chargeability and SPT-N values. The weights of all parameters are also similar for both chargeability and SPT-N value. (2) Fines (clay) and water content have negative contribution, whereas sand has a positive contribution in resistivity values. The weights of different parameters are negative in sign when compared to that of SPT and IP. (3) The behaviour of dependent variable (IP chargeability and SPT-N) with respect to that of independent parameters is similar.

For illustration sake we include Figure 3 *a-c* to show as to how the sand and water content as independent parameters influence prediction of dependent functions, SPT-N, chargeability and resistivity. Similarly, the influence of fines and water content on dependent functions can also be demonstrated (those plots are not included here). Thus the multi-regression results clearly confirm our initial contention that grain size (sand), fines (shale content) and water content influence both geoelectric (ERI and IPI) and geotechnical (SPT) measurements.

In order to achieve a conjunctive use of cost-effective geoelectric imaging and costly and invasive site geotechnical tests in a minimal manner, it demands a careful objective analysis of independent influencing factors on both these different datasets. Multiple regression analysis shows that both ERI/IPI and SPT are affected by sand, fines and water content. Based on prediction results, IPI and SPT are affected by grain size and water content in a similar way. However, the choice of ERI/IPI is site-dependent and geoelectric imaging can be adopted for geotechnical site characterization in a cost-effective manner.

1. Bowles, J. S., *Foundation Analysis and Design*, McGraw Hill International, Singapore, 2001, 5th edn, p. 171.
2. Murthy, V. N. S., *Soil Mechanics and Foundation Engineering*, CBS Publisher and Distributors, 2008, p. 1043.
3. Gautam, P. K., Sastry, R. G. and Mondal, S. K., The utility of multi-electrode resistivity data in geotechnical investigations – a case study. In 20th Symposium on the Application of Geophysics to Engineering and Environmental Problems, 2007, pp. 731–737.
4. Cocker, J. O., Integration of geophysical and geotechnical methods to site characterization for construction work at the school of management area, Lagos State Polytechnic, Ikorodu, Lagos, Nigeria. *Int. J. Energy Sci. Eng.*, 2015, **1**(2), 40–48.
5. Terzaghi, K. and Peck, R. B., *Soil Mechanics in Engineering Practice*, John Wiley, New York, 3rd edn, 1996, p. 549.
6. Schön, J. H., Physical properties of rocks: fundamentals and principles of petrophysics. In *Handbook of Geophysical Exploration*, Elsevier, New York, 1996, vol. 18, p. 583.
7. Rucker, D. F. and Noonan, G. E., Using marine resistivity to map geotechnical properties: a case study in support of dredging the Panama Canal. *Near Surf. Geophys.*, 2013, **11**(6), 625–637.

8. Sudha, K., Israil, M., Mittal, S. and Rai, J., Soil characterization using electrical resistivity tomography and geotechnical investigations. *J. Appl. Geophys.*, 2009, **67**, 74–79.
9. Abidin, M. H. Z., Saad, R., Ahmad, F., Wijeyesekera, D. C. and Baharuddin, M. F. T., Correlation analysis between field electrical resistivity value (ERV) and basic geotechnical properties (BGP). *Soil Mech. Found. Eng.*, 2014, **51**(3), 117–125.
10. Siddiqui, F. I. and Osman, S. B., Integrating geo-electrical and geotechnical data for soil characterization. *Int. J. Appl. Phys. Math.*, 2012, **2**(2), 104–106.
11. Siddiqui, F. I. and Osman, S. B., Simple and multiple regression models for relationship between electrical resistivity and various soil properties for soil characterization. *Environ. Earth Sci.*, 2013, **70**, 259–267.
12. Ranjan, G., and Rao, A. S. R., *Basic and Applied Soil Mechanics*, New Age International Publishers, 2000, p. 762.
13. Loke, M. H. and Barker, R. D., Least-squares deconvolution of apparent resistivity pseudosections. *Geophysics*, 1995, **60**, 1682–1690.
14. Rai, S. K., Singh, S. K. and Krishnaswami, S., Chemical weathering in the plain and peninsular sub-basins of the Ganga: impact on major ion chemistry and elemental fluxes. *Geochim. Cosmochim. Acta*, 2010, **74**, 2340–2355.
15. Singh, S., Parkash, B., Rao, M. S., Arora, M. and Bhosle, B., Geomorphology, pedology and sedimentology of the Deoha/Ganga–Ghaghara interfluvies, Upper Gangetic Plains (Himalayan Foreland Basin) – extensional tectonic implications. *Catena*, 2006, **67**, 183–203.
16. Srivastava, P., Pal, D. K., Aruche, K. M., Wani, S. P. and Sahrawat, K. L., Soils of the Indo-Gangetic Plains: a pedogenic response to landscape stability, climatic variability and anthropogenic activity during Holocene. *Earth Sci. Rev.*, 2015, **140**, 54–71.
17. Parkash, B., Kumar, S., Rao, M. S., Giri, S. C., Kumar, C. S., Gupta, S. and Srivastava, P., Holocene tectonic movements and stress field. *Curr. Sci.*, 2000, **79**(4), 438–449.
18. Pazdirek, O. and Blaha, V., Examples of resistivity imaging using ME-100 resistivity field acquisition system. In EAGE 58th Conference and Technical Exhibition Extended abstr., Amsterdam, 1996.
19. Loke, M. H., Electrical imaging surveys for environmental and engineering studies – a practical guide to 2D and 3D surveys. A Report, 2000, p. 60.
20. Press, W. H., Teukolsky, S. A., Vetterling, W. T. and Flannery, B. P., *Numerical Recipes – The Art of Scientific Computing*, Cambridge University Press, New Delhi, 2007, 3rd edn, p. 1195.
21. Gujarati, D. N., Porter, D. C. and Gunasekar, S., *Basic Econometrics*, McGraw Hill Education (India), New Delhi, 2012, 5th edn, p. 886.

ACKNOWLEDGEMENTS. S.C. thanks the Ministry of Human Resource Development, Government of India for a research fellowship.

Received 27 June 2017; revised accepted 29 November 2017

doi: 10.18520/cs/v114/i09/1946-1952